UNIVERSITÉ DE GENÈVE

Archive ouverte UNIGE
https://archive-ouverte.unige.ch

Article scientifique | Article | 2025

Published version | Open Access

This is the published version of the publication, made available in accordance with the publisher's policy.

Enhanced intracranial aneurysm development in a rat model of polycystic kidney disease

Cayron, Anne France Judith; Morel, Sandrine; Azam, Maral; Haemmerli, Julien; Aoki, Tomohiro; Bijlenga, Philippe Alexandre Pierre; Allémann, Eric; Kwak, Brenda

How to cite

CAYRON, Anne France Judith et al. Enhanced intracranial aneurysm development in a rat model of polycystic kidney disease. In: Cardiovascular research, 2025, p. cvaf063. doi: 10.1093/cvr/cvaf063

This publication URL: https://archive-ouverte.unige.ch/unige:185187
Publication DOI: 10.1093/cvr/cvaf063

© The author(s). This work is licensed under a Creative Commons Attribution-NonCommercial (CC BY-NC 4.0) https://creativecommons.org/licenses/by-nc/4.0

ESC European Society of Cardiology

Cardiovascular Research (2025) **00**, 1–14
https://doi.org/10.1093/cvr/cvaf063

Enhanced intracranial aneurysm development in a rat model of polycystic kidney disease

Anne France Cayron [1,2,3,4], Sandrine Morel [1,2,5,6], Maral Azam[1,2], Julien Haemmerli[5], Tomohiro Aoki[7], Philippe Bijlenga [5], Eric Allémann [3,4,8], and Brenda Renata Kwak [1,2]*

[1]Department of Pathology and Immunology, University of Geneva, Rue Michel-Servet 1, Geneva CH-1211, Switzerland; [2]Geneva Center for Inflammation Research, University of Geneva, Rue Michel-Servet 1, Geneva CH-1211, Switzerland; [3]School of Pharmaceutical Sciences, University of Geneva, Geneva, Switzerland; [4]Institute of Pharmaceutical Sciences of Western Switzerland, University of Geneva, Geneva, Switzerland; [5]Division of Neurosurgery, Department of Clinical Neurosciences, Faculty of Medicine, Geneva University Hospitals and University of Geneva, Geneva, Switzerland; [6]HUG NeuroCentre, Geneva University Hospitals, Geneva, Switzerland; [7]Department of Pharmacology, The Jikei University School of Medicine, Tokyo, Japan; and [8]Small Animal Preclinical Imaging Platform, Faculty of Medicine, University of Geneva, Geneva, Switzerland

Received 9 June 2024; revised 9 December 2024; accepted 23 February 2025; online publish-ahead-of-print 18 April 2025

Time of primary review: 67 days

Aims Polycystic kidney disease (PKD) patients have a high intracranial aneurysms (IAs) incidence and risk of rupture. The mechanisms that make PKD patients more vulnerable to IA disease are still not completely understood. The PCK rat is a well-known PKD model and has been extensively used to study cyst development and kidney damage. Here, we used this rat model to study IA induction and vulnerability.

Methods and results IAs were induced in wild-type (WT) and PCK rats and their incidence was followed. Variation in the anatomy of the circle of Willis was studied in PCK rats and PKD patients. Immunohistochemistry was performed in rat IAs and in human ruptured and unruptured IAs from patients enrolled in the @neurIST observational cohort. An increased frequency of fatal aortic dissection was unexpectedly observed in PCK rats, which was due to modifications in the elastic architecture of the aorta in combination with the induced hypertension. Interestingly, IAs developed faster in PCK rats compared to WT rats. Variations in the anatomy of the circle of Willis were identified in PCK rats and PKD patients, a risk factor that may (in part) explain the higher IA incidence found in these groups. At 2 weeks after induction, the endothelium of IAs from PCK rats showed a decrease in the tight junction proteins zonula occludens-1 and claudin-5. Furthermore, the Type III collagen content was lower in IAs of PCK rats at 4 weeks post-surgery. The decrease in tight junction proteins was also observed in the endothelium of human ruptured IAs compared to unruptured IAs.

Conclusion Our study showed that PCK rats are more sensitive to IA induction. Variations in the anatomy of the circle of Willis and impaired regulation of tight junction proteins might put PCK rats and PKD patients more at risk of developing vulnerable IAs.

Downloaded from https://academic.oup.com/cardiovascres/advance-article/doi/10.1093/cvr/cvaf063/8115994 by guest on 21 May 2025

* Corresponding author. Tel: +41 22 379 5666, E-mail: Brenda.KwakChanson@unige.ch

© The Author(s) 2025. Published by Oxford University Press on behalf of the European Society of Cardiology.
This is an Open Access article distributed under the terms of the Creative Commons Attribution-NonCommercial License (https://creativecommons.org/licenses/by-nc/4.0/), which permits non-commercial re-use, distribution, and reproduction in any medium, provided the original work is properly cited. For commercial re-use, please contact reprints@oup.com for reprints and translation rights for reprints. All other permissions can be obtained through our RightsLink service via the Permissions link on the article page on our site—for further information please contact journals.permissions@oup.com.

Graphical Abstract

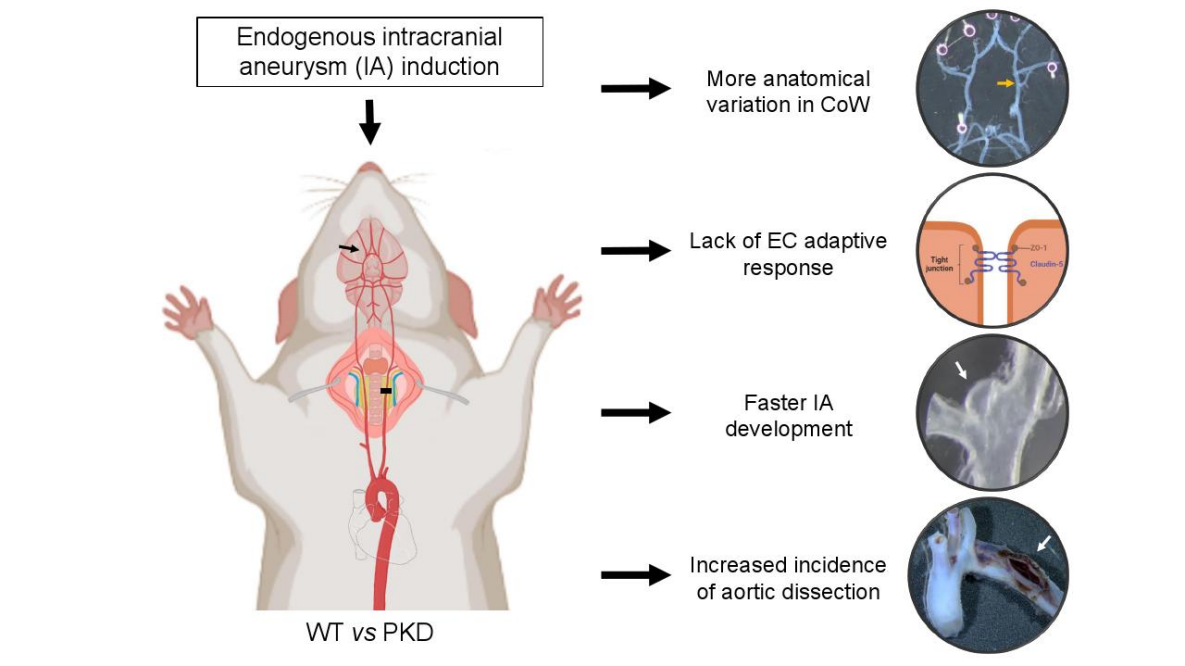

Keywords Polycystic kidney disease • Intracranial aneurysm • Rats • Circle of Willis • Tight junctions

1. Introduction

Intracranial aneurysms (IAs) are abnormal enlargements of the lumen of arteries in the circle of Willis (CoW), which affects 2–5% of the population.[1,2] IA rupture leading to subarachnoid haemorrhage (SAH) is fatal in 25–50% of the cases.[3] Unruptured IAs can be preventively treated, but these interventions are rather perilous with ∼4.2% risk of mortality and ∼3.6% risk of morbidity.[4] Thus, it is essential to identify unstable IAs prone to rupture accurately.

IAs typically develop at bifurcations within the CoW, an arterial network responsible for supplying blood to the brain.[5] The CoW is composed of the anterior cerebral arteries (ACA), the anterior communicating artery (ACOM), the internal carotid arteries (ICA), the middle cerebral arteries (MCA), the posterior communicating arteries (PCOM), the posterior cerebral arteries (PCA), and the basilar artery (BA). The CoW is conserved across many species[6] and is divided in the anterior and posterior circulations fed by the ICAs and BA, respectively.[7] Many morphological variations in the CoW have been found in the general population.[8] Those variations modify the haemodynamics and the wall shear stress applied to endothelial cells (ECs).[9] Wall shear stress is known to have a critical role in the initiation of IAs,[5] and CoW variations have been correlated with this process.[10,11]

Polycystic kidney disease (PKD) is a genetic disease characterized by an excessive development of renal cysts, which deteriorates kidney function and may lead to organ failure.[12] There are two distinct types of PKD: autosomal recessive (ARPKD), a rare form diagnosed in infancy, and autosomal dominant (ADPKD), the most common form, typically diagnosed in adulthood due to later onset of symptoms.[13] Interestingly, ADPKD has been associated with a high IA incidence and risk of rupture.[12,14] Furthermore, several case reports have described IAs in ARPKD patients,[15–19] despite the shortened life expectancy of these patients. The improved medical management of the comorbidities associated with ARPKD might increase the life expectancies of these patients and the frequency of IAs in ARPKD patients.[19] PKD patients, affected by the dominant or recessive form, carry a mutation in the PKD1, PKD2, or PKHD1 genes affecting the function of primary cilia.[20] In ECs lining the lumen of the arterial wall, primary cilia act as mechano-sensors of blood flow.[5] We have recently shown *in vitro* that primary cilia dampen the endothelial response to an aneurysmal pattern of disturbed flow.[21] The tight junction protein zonula occludens-1 (ZO-1) was identified as a central regulator of primary cilia-dependent junction integrity.[21] As tight junctions control endothelial permeability, dysfunctional endothelial tight junctions have been associated with multiple vascular diseases.[22] Claudin-5 (CLDN5) is a tight junction protein highly expressed in intracranial endothelium and plays a key role in maintaining the blood brain barrier.[23,24] We hypothesize that a decrease of tight junction proteins might explain why PKD patients develop IAs more frequently and these IAs are more at risk to rupture.

In this study, PCK rats were used as model of PKD and compared to wild-type (WT) rats. The PCK rat is a model of ARPKD, with a mutation in the homologous gene of PKHD1, and which can be used as model of ADPKD as this model shares several key features with human ADPKD.[25] The PCK rat carries non-functional primary cilia and has been extensively used to study cyst development and hepatorenal damage.[26] However, PCK rats were never used to study IA development. We found that IAs developed faster in PCK rats compared to WT rats. Moreover, variations in the anatomy of the CoW were identified in PCK rats and ADPKD patients, a risk factor that may (in part) explain the high IA incidence found in these groups. At 2 weeks after induction, the endothelium of IAs from PCK rats showed a lower content in tight junction proteins ZO-1 and CLDN5, compared to WT rats. Moreover, the content of Type III collagen was lower in IAs of PCK rats at 4 weeks post-surgery. The reduced tight junction protein expression was also observed in the endothelium of human ruptured IAs compared to unruptured IAs of patients enrolled in the @neurIST study.

Downloaded from https://academic.oup.com/cardiovascres/advance-article/doi/10.1093/cvr/cvaf063/8115994 by guest on 21 May 2025

2. Methods

2.1 Rat IA model

The experiments were approved by the Swiss federal and cantonal veterinary authorities (license GE21519A) and performed according to the Guide for the Care and Use of Laboratory Animals and the Swiss national animal protection laws. The animal experiments complied with the National Institute of Health's Guide for the Care and Use of Laboratory Animals and the Animal Research Reporting *In Vivo* Experiments (ARRIVE) guidelines.

Five- to 9-week-old male WT and PCK (PCK/CrljCrl-Pkhd1^{Pck}/CRL) CD Sprague-Dawley rats were obtained from Charles River Laboratories. The animals were randomly selected and placed in cages (2–5 animals per cage). Animals were marked with tail marks and the acclimatization phase lasted at least 7 days. Rats were held in an enriched environment with *ad libitum* access to water and food. After acclimatization, rats were accommodated to the restrainer chamber to measure systolic blood pressure (BP) for 3 consecutive days. The protocol to induce IAs was applied to 30 WT and 33 PCK rats. Eight WT and 12 PCK controls rats did not undergo any surgery, were fed with a normal diet and were killed in parallel with rats exposed to the IA induction protocol. All animals were monitored and daily scored for general well-being during the first 3 days post-surgery and then twice a week until the end of the experiment.

Following the well-known protocol of Aoki *et al.*[27,28] IAs were induced at the right olfactory artery (OA) and ACA bifurcation. Briefly, under general anaesthesia with inhalation of isofluorane (4% for induction, 2% for maintenance), haemodynamic stress was increased on the right half of the CoW by ligation of the left common carotid artery (LCCA). Hypertension was induced by ligation of the left renal artery in combination with a high salt diet (8%). The arterial wall was weakened by addition of 0.12% β-aminopropionitrile (BAPN) to the diet. To reduce pain, two subcutaneous injections of buprenorphine (0.05 mg/kg in 100 µL) were given 30 min before surgery and 4–6 h later. Buprenorphine was also added to the drinking water (0.05 mg/kg) for 2 days post-surgery. Systolic BP was regularly measured by the tail-cuff method. Animals were placed in the restrainer chamber at 34°C, and BP was measured using the MRBP tail-cuff BP multi-channel system (IITC Life Science) after 5 min of acclimatation. Results were expressed as the mean of three measurements for each animal. Animals were euthanized at 1–8 weeks post-surgery by intraperitoneal injection of a lethal dose of ketasol (100 mg/kg) and xylazine (10 mg/kg) and bloodletting. Any animal that died during the experiment was meticulously examined to determine the cause of death.

2.2 Clinical and radiological data

Patients have been recruited at the Geneva University Hospitals. The inclusion criteria were as follows: (i) IA identified on the basis of angiographic appearance (3D-digital subtraction angiography, 3D-magnetic resonance angiogram, or 3D-computed tomography angiogram) as well as availability of surgical documentation; (ii) age older than 18 years; (iii) patient provided informed consent. The exclusion criteria were as follows: (i) lack of angiographically proven IA on 3D-digital subtraction angiography, 3D-magnetic resonance angiogram, or 3D-computed tomography angiogram; (ii) failure to contribute to clinical data; and (iii) refusal to provide informed consent. This study is in accordance with the Helsinki Declaration of the World Medical Association and was approved by the Geneva State Ethics Commission for Research as part of the @neurIST study (PB 2022-00426 previously PB_2018-0073 and 07-056). All patients approved for the use of their data and biological samples in the field of cerebrovascular research.

For the analysis of CoW organization, magnetic resonance images (MRIs) of 16 ADPKD patients were retrieved from the @neurIST cohort. MRIs of 16 matched non-PKD patients were also selected from the @neurIST cohort such that there were no differences between the two groups in terms of sex, positive family history for IAs and IA multiplicity. In a larger cohort of non-PKD patients, MRIs of patients with ($n = 24$) and without a history of aneurysmal SAH ($n = 33$) were also retrieved from the @neurIST cohort. For the purpose of the analysis, a time of flight (TOF) sequence was used. CoW of the PKD ($n = 16$) and non-PKD patients ($n = 16$) were classified by three blinded observers using the TOF images according to the classification presented in Supplementary material online, *Figure S1* (see Supplementary material online). CoW of the patients with ($n = 24$) and without a history of aneurysmal SAH ($n = 33$) were classified by two blinded observers. This classification was adapted from Kızılgöz *et al.*[7] Variants A represent a complete CoW and was the most common anatomical configuration observed. Other variants correspond to the major incomplete configurations of the CoW identified in our cohort and are categorized based on variations in either the anterior or posterior part of the CoW.

2.3 Human IA samples

For histological studies, 38 unruptured and 19 ruptured human IA domes localized at the MCA in non-PKD patients were retrieved from the Swiss AneuX biobank.[29] Human saccular IAs samples were obtained and processed as previously described.[29]

This study is in accordance with the Helsinki Declaration of the World Medical Association and was approved by the Ethical Committee of the Geneva University Hospitals, Geneva, Switzerland, as part of the @neurIST study (Geneva State Ethics Commission for Research PB 2022-00426 previously PB_2018-0073 and 07-056). All patients signed the consent forms and approved for the use of their data and biological samples in the field of cerebrovascular research.

2.4 Rat samples

Rats were euthanized under anaesthesia with an intraperitoneal injection of ketarom (ketasol 100 mg/kg and xylazine 10 mg/kg) and transcardially perfused with 4% paraformaldehyde. The CoW, aortic arch, and right kidney were collected from all rats, fixed overnight in 4% paraformaldehyde and transferred to a 30% sucrose-phosphate-buffered saline solution until complete dehydration. Prior to sample embedding, the complete CoW, right OA-ACA bifurcation and aortic arches of all rats were imaged using a Stemi 508 stereo microscope (Carl Zeiss). Right kidneys were weighed. Right OA-ACA bifurcation, aortic arch and right kidney of all animals were embedded in OCT compound, snap frozen, and stored at −80°C.

Images of the CoW of all WT ($n = 38$) and PCK ($n = 44$) rats were analysed using the ImageView software (ImageView v4.11.18709.20210403) to study their anatomical organization. The CoW of one PCK rat that died prematurely was too damaged and was not studied. Aortic arches of animals that died prematurely were studied to find potential anomalies that could have caused the death of the animal.

2.5 Histology, immunohistochemistry, and immunofluorescence

Human IA samples were sectioned at 5 µm and conserved at 4°C. Immunoreactivity was retrieved by pressure cooker treatment (3 min) in citrate buffer. ECs were immunolabelled for CD31 (#DLN-33600, Dianova, 1/25), ZO-1 (#61-7300, Invitrogen, 1/100), and CLDN5 (#PAB27037, Abnova, 1/1000). Labellings were visualized using secondary antibody coupled to streptavidin-biotin peroxidase complex and 3,3′-diamino-benzidine chromophore using the EnVision Flex system (#K8023, DAKO) or the VECTASTAIN Kit (#PK-7800, Vector Laboratory) combined with ImmPACT DAB Substrate Kit (#SK-4105, Vector Laboratory). Hemalun (#1.09249, Merck) was used as counterstaining. Samples were mounted with Aquatex (#108562, Sigma Aldrich). Stainings were performed on consecutive sections.

The right OA-ACA bifurcations, aortic arches, and right kidneys of rats were sectioned at 6 µm and conserved at −20°C. Kidney sections were stained with haematoxylin/eosin. Aortic arch sections were stained for Martius Scarlet blue to visualize fibrin and Victoria blue to study the elastic architecture. For immunohistochemistry, right OA-ACA bifurcation sections were fixed in 4% paraformaldehyde for 15 min, permeabilized in ice-cold 100% methanol for 3 min and blocked with 2% bovine serum albumin (#A1391, AppliChem) or 10% normal goat serum (#S-1000, Vector

Downloaded from https://academic.oup.com/cardiovascres/advance-article/doi/10.1093/cvr/cvaf063/8115994 by guest on 21 May 2025

Laboratories) for 15 min. ECs were immunolabelled for CD31 (#DLN-33600, Dianova, 1/100), ZO-1 (#61-7300, Invitrogen, 1/100), CLDN5 (#PAB27037, Abnova, 1/200), and CD68 (#MCA341R, BioRad, 1/100). A FITC-conjugated goat anti-rabbit antibody (#711-095-152, Jackson Lab, 1/100) or FITC-conjugated goat anti-mouse antibody (#115-095-003, Jackson Lab, 1/100) was used for signal detection. Nuclei and internal elastic lamina were counterstained with 4′,6-diamidino-2-phenylindol (DAPI) and 0.003% Evans Blue, respectively. Samples were mounted with Vectashield antifade mounting medium (#H-1000-10, Vector Laboratories). Right OA-ACA bifurcation sections were also stained with Picrosirius Red. All stainings were performed on consecutive sections.

2.6 Image analysis

Stainings on human IA sections, rat aortic arches, and kidneys were scanned at 10× magnification using the Axio Scan.Z1 automated slide scanner (Carl Zeiss) and images were processed by a blinded observer using the Zen 2 software (Version 3.4.91, Carl Zeiss). Using the ImageJ (FIJI) software (Java 1.8.0, NIH), CD31, ZO-1, and CLDN5 staining on human IA sections was quantified by a blinded observer at five different locations along the endothelium using previously established methods.[21] Results were expressed as the mean of the five measurements for each sample. Picrosirius red staining on rat right OA-ACA bifurcation sections were examined using polarized light on the Olympus VS120 microscope and processed using QuPath software. Yellow-red and green birefringence were utilized to distinguish Type I and Type III collagen fibres, respectively. Collagens were expressed as percentages of the total wall area. Immunostainings on rat right OA-ACA bifurcation sections were imaged using the epifluorescent Zeiss Axiocam Imager Z1 (Carl Zeiss) equipped with an AxioCam 506 mono camera (Carl Zeiss). Images at a high optical resolution (0.093µm/pixel) were processed and analysed using the Zen 2 software (Version 3.4.91, Carl Zeiss). Similar to the human sections, CD31, ZO-1, and CLDN5 stainings were quantified by a blinded observer at five different locations along the endothelium at the level of the right OA-ACA bifurcation, where the IA developed, and in the ACA. Results were expressed as the mean of the five measurements for each sample. The number of CD68 positive cells were counted by a blinded observer at the level of the right OA-ACA bifurcation and in the ACA.

2.7 Statistical analysis

Statistical analysis was performed using GraphPad Prism (Version 10.1.1, GraphPad). The distribution of the data was assessed by the D'Agostino-Pearson Normality test. Normally distributed data are expressed as mean ± SD. Data with non-normally distributed data (including $n < 8$) are expressed as median ± interquartile range. The presence of outliers was identified using the ROUT method ($Q = 1\%$) and removed from the statistical analysis if present. The difference between the means of two independent groups with normally distributed data was analysed using a one- or two-tailed Student's *t*-test. One-tailed *t*-test was used when a difference in a specific direction was expected. The difference between the median of two independent groups with non-normally distributed data was analysed using a Mann–Whitney *U* test. Difference between the median of multiple groups with non-normally distributed data was analysed using a Kruskal–Wallis test and Dunn's multiple comparisons test. Comparison of distributions has been performed using the Fisher's exact test. $P < 0.05$ indicates statistical significance: $^{*}P < 0.05$, $^{**}P < 0.01$, $^{***}P < 0.001$, and $^{****}P < 0.0001$.

3. Results

3.1 WT and PCK rats display similar increases in systolic BP

To induce IAs, young (6–10 weeks) WT and PCK rats were exposed to ligation of the LCCA and the left renal artery followed by a high salt diet enriched with BAPN. The body weight of WT and PCK rats were similar (~320 g) at the time of surgery and although PCK rats seemed to gain less weight than WT rats these differences were not significant during the full experiment (*Figure 1A*). As expected, haematoxylin/eosin staining on the right kidney revealed the presence of cysts in PCK rats (*Figure 1B*) which were absent in WT rats (*Figure 1C*). Likewise, we observed increased weight of the right kidney in control PCK rats ($P = 0.0010$) (*Figure 1D*) and in PCK rats after surgery ($P < 0.0001$) (*Figure 1E*) compared to control WT rats and WT rats after surgery. Finally, the systolic BP was carefully monitored before and after surgery. In both WT and PCK rats, the systolic BP raised in 1 week by 30 mmHg reaching ~160 mmHg after which it remained elevated, thus confirming the induced hypertension in WT and PCK rats in response to renal artery ligation and high salt diet (*Figure 1F*). Despite the polycystic kidneys of PCK rats, no differences in blood pressure were observed between WT and PCK rats.

3.2 PCK rats show decreased survival

We originally planned to compare IA development in groups of young WT and PCK rats for up to 8 weeks post-surgery. While the survival rate of WT rats was 100% until 6 weeks post-surgery with thereafter a slight decrease to 90% at 8 weeks, a sudden increase in mortality of PCK rats was observed at 3 weeks post-surgery (*Figure 2A*). The survival rate of PCK rats even dropped below 50% at 4 weeks post-surgery. Thus, in accordance with 3R principles, we decided to stop the experiment with PCK rats at maximum 4 weeks post-surgery. In consequence, WT rats were killed at 2, 4, and 8 weeks post-surgery, as planned, and the PCK rats at 1, 2, 3, and 4 weeks post-surgery. Autopsy of WT and PCK rats that died prematurely during the experiment (3 out of 30 WT and 10 out of 33 PCK rats) revealed the presence of thoracic haemorrhage. Microscopic observation revealed the presence of dissection in the aortic arch (*Figure 2B*) as cause of the thoracic haemorrhage. Disruption of elastic laminae and presence of erythrocytes and fresh fibrin within the arterial wall of the aortic arch, creating a pseudolumen, confirmed the aortic dissection diagnosis (*Figure 2C–E*).

To better understand the aortic wall changes leading to the aortic dissection, the elastic architecture was studied at different locations in the aortic arch (*Figure 2F*) of five control WT and PCK rats and five WT and four PCK rats killed 4 weeks post-surgery. We observed three types of elastic architecture (*Figure 2G*): Aortic walls containing straight, thick elastic lamellae and dense elastic fibres were classified as Stage 1. Aortic walls containing straight, thick elastic lamellae and not very dense elastic fibres were classified as Stage 2. Aortic walls containing thin or undulated elastic lamellae and sparse elastic fibres were classified as Stage 3. While the elastic architecture downstream of the left subclavian artery was identical and mostly normal (80% Stage 1) in the WT and PCK rats without surgery (*Figure 2H*), the elastic architecture was more severely affected at the same location at 4 weeks post-surgery in PCK rats compared to WT rats ($P < 0.0001$) (*Figure 2I*). This different response of PCK rats to the IA induction protocol as compared to WT rats was even more evident at the level of the ascending aorta and in the aortic wall between the bifurcations of the brachiocephalic trunk and the LCCA with elastic architecture classified as Stages 2 or 3 in all PCK rats at 4 weeks post-surgery (see Supplementary material online, *Figure S2A–D*). In general, the elastic fibre density tended to be decreased in PCK rats at 4 weeks post-surgery at all three locations in the aortic arch (see Supplementary material online, *Figure S2E–G*). The severe alteration of the elastic architecture in the aortic arch of PCK rats compared to WT rats might explain the increased frequency of aortic dissections observed in PCK rats 4 weeks post-surgery.

3.3 PCK rats display faster IA development

The right OA-ACA bifurcation from WT (*Figure 3A* and *B*) and PCK rats (*Figure 3C* and *D*) were closely examined to find IAs at the various time points post-surgery. Meticulous observation under the dissection microscope revealed the presence of bulging in WT and PCK rats (*Figure 3A* and *C*). Immunofluorescent staining confirmed the bulging and revealed the presence of internal elastic lamina disruption (*Figure 3B* and *D*), which

Downloaded from https://academic.oup.com/cardiovascres/advance-article/doi/10.1093/cvr/cvaf063/8115994 by guest on 21 May 2025

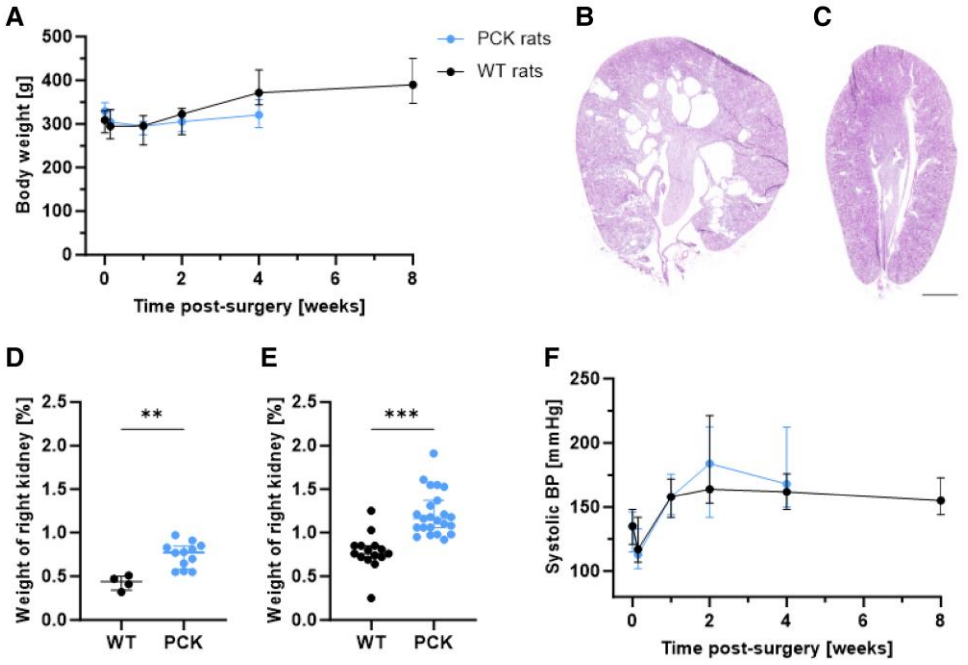

Figure 1 WT and PCK rats have similar body weight and BP. (*A*) Body weight evolution of WT ($n = 27$) and PCK rats ($n = 23$) following surgery to induce IAs. Kruskal–Wallis test with Dunn's multiple comparisons test between WT and PCK rats. (*B* and *C*) Haematoxylin/eosin staining of a right kidney section of a PCK (*B*) and a WT (*C*) rat without surgery. Scale bar, 2 mm. (*D* and *E*) Weight of right kidney of control WT ($n = 4$) and PCK ($n = 12$) rats (*D*) and WT ($n = 15$) and PCK ($n = 23$) rats after surgery (*E*). Values are expressed as percentage of body weight. Two-tailed Mann–Whitney *U* test. (*F*) Systolic BP evolution of WT ($n = 27$) and PCK ($n = 23$) rats following surgery to induce IAs. Kruskal–Wallis test with Dunn's multiple comparisons test between WT and PCK rats. $^{**}P < 0.01$, $^{***}P < 0.001$.

is a characteristic of IAs. WT rats showed a progressive increase in IA occurrence with time after surgery leading to 82% of rats having an IA at 8 weeks post-surgery (*Figure 3E*). Interestingly, PCK rats displayed at 2 weeks post-surgery enhanced IA development ($P = 0.0070$) (*Figure 3F*) and the maximal IA induction of 86% was already reached at 3 weeks post-surgery in PCK rats, half of the time needed for WT rats (*Figure 3G*). No difference in IA size (*Figure 3H*) and length of internal elastic lamina disruption (*Figure 3I*) were observed between WT and PCK rats at similar time points post-surgery. Thus, IA development was faster in PCK rats, which may be due to the absence of functional primary cilia to dampen the endothelial response to disturbed blood flow.

3.4 Anatomical variations in the CoW of PCK rats and PKD patients

The CoW is conserved across many species and shows a high degree of similarity between humans and rats[6] (see Supplementary material online, *Figure S3*). Disturbed blood flow patterns play a critical role in the initiation of IAs.[5] Anatomical variations in the CoW have been associated with IA formation;[10,11] however, the role of primary cilia in this process remains to be investigated. Three frequent variations in the organization of the CoW were observed in the rat, i.e. an additional MCA bifurcation (*Figure 4A*), an additional ACA bifurcation (*Figure 4B*), and the presence of an ACOM (*Figure 4C*). These variants were more frequently observed in PCK rats than in WT rats ($P = 0.0035$, $P = 0.0101$, and $P = 0.0137$, respectively) (*Figure 4D–F*). Therefore, we decided to compare the anatomical variability of the CoW between PKD and non-PKD patients. The @neurIST database contained MRIs of 16 ADPKD patients. Sixteen non-PKD patients were selected from the same database based on matching for sex, positive family history for IAs and IAs multiplicity. As presented in *Table 1*, this clinical data from ADPKD and non-PKD patients were not different. Human CoW were classified using MRIs (see Supplementary material online, *Figure S1*) and differences were separated for the anterior (*Figure 4G*) and posterior (*Figure 4H*) part of the CoW. Anterior and posterior CoW of PKD patients were less often classified as Type A which corresponds to the predominant CoW anatomical morphology in non-PKD patients ($P < 0.0001$ and $P = 0.0001$). Additional ACOM or ACA were more frequently observed in the anterior part of the CoW from PKD patients than non-PKD patients. Absence or hypoplasia of the ACA was observed in none of the PKD patients while this variant was observed in 12.5% of non-PKD patients. Dominance of one PCOM was observed less frequently and absence or hypoplasia of both PCOM was observed more frequently in PKD patients than in non-PKD patients. In a larger cohort of non-PKD patients, the organization of the CoW differed in patients with a history of aneurysmal SAH compared to patients with no history of SAH (see Supplementary material online, *Figure S4*). Interestingly, variations of the CoW observed more frequently in PKD patients, such as additional ACOM or ACA or absence or hypoplasia of both PCOM, were also more common in patients with a history of aneurysmal SAH. Altogether, we observed an increased number of anatomical variations in CoW of both PCK rats and PKD patients. Notably, the presence of additional ACOM and ACA was observed in both groups. This suggests that the absence of functional endothelial primary cilia might lead to altered embryologic development of the circulatory system.

3.5 Absence of increase in tight junction proteins in IAs of PCK rats

In an unbiased transcriptomics *in vitro* study, we previously identified ZO-1 as a central regulator of primary cilia-dependent tight junction integrity and endothelial permeability.[21] To investigate the relation between primary cilia and endothelial junction integrity *in vivo*, we examined different EC

Downloaded from https://academic.oup.com/cardiovascres/advance-article/doi/10.1093/cvr/cvaf063/8115994 by guest on 21 May 2025

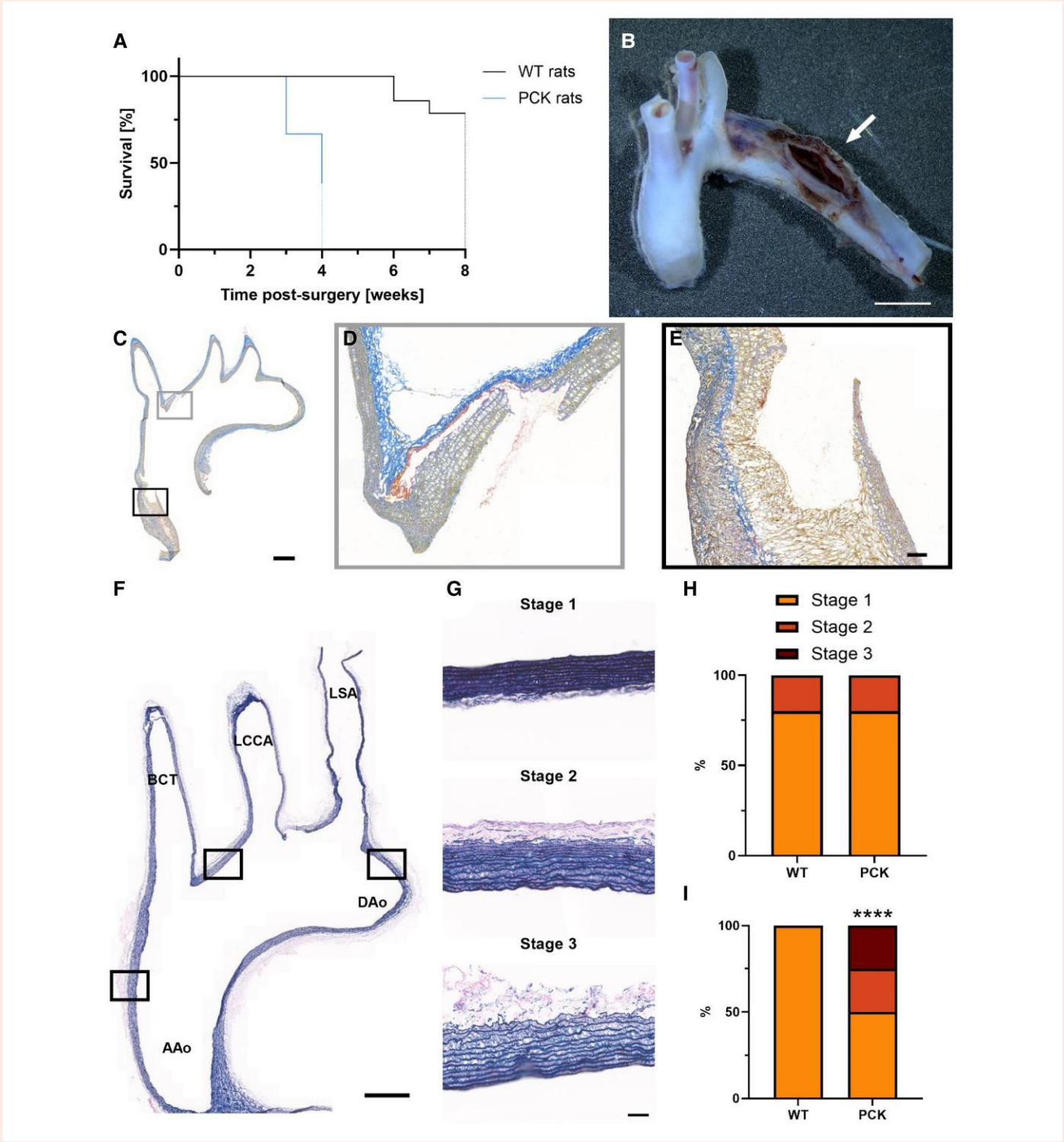

Figure 2 Reduced survival of PCK rats due to aortic dissection. (*A*) Survival rate of WT ($n = 30$) and PCK rats ($n = 33$) following surgery to induce IAs. Dotted lines indicate rats killed at the end of the experiment. (*B*) Representative image of an aortic arch from a PCK rat that prematurely died 3 weeks post-surgery. Scale bar, 3 mm. Arrow indicates the site of dissection. (*C*) Martius Scarlet blue staining of an aortic arch section of a WT rat that prematurely died 6 weeks post-surgery. Nuclei are stained in brown, fibrin in red, erythrocytes and fresh fibrin in yellow, and white blood cells and collagen in blue. Scale bar, 1 mm. Grey (*D*) and black (*E*) panels are magnifications showing the vessel wall deterioration and the infiltration of blood into the vessel wall. Scale bar, 0.1 mm. (*F*) Victoria blue staining of an aortic arch section from a PCK rat killed 4 weeks post-surgery illustrating the three locations at which elastic architecture was studied. Scale bar, 1 mm. Aao, ascending aorta; DAo, descending aorta; BCT, brachiocephalic trunk; LCCA, left common carotid artery; LSA, left subclavian artery. (*G*) Representative Victoria blue staining images of Stages 1, 2, and 3. (*H* and *I*) Classification of the elastic architecture downstream of the LSA in the aortic arch (location indicated in *D*) of five control WT and five control PCK rats (*H*) and five WT and four PCK rats killed 4 weeks post-surgery (*I*). Yellow, Stage 1; orange, Stage 2; and dark red, Stage 3. Fisher's exact test. ****$P < 0.0001$.

Downloaded from https://academic.oup.com/cardiovascres/advance-article/doi/10.1093/cvr/cvaf063/8115994 by guest on 21 May 2025

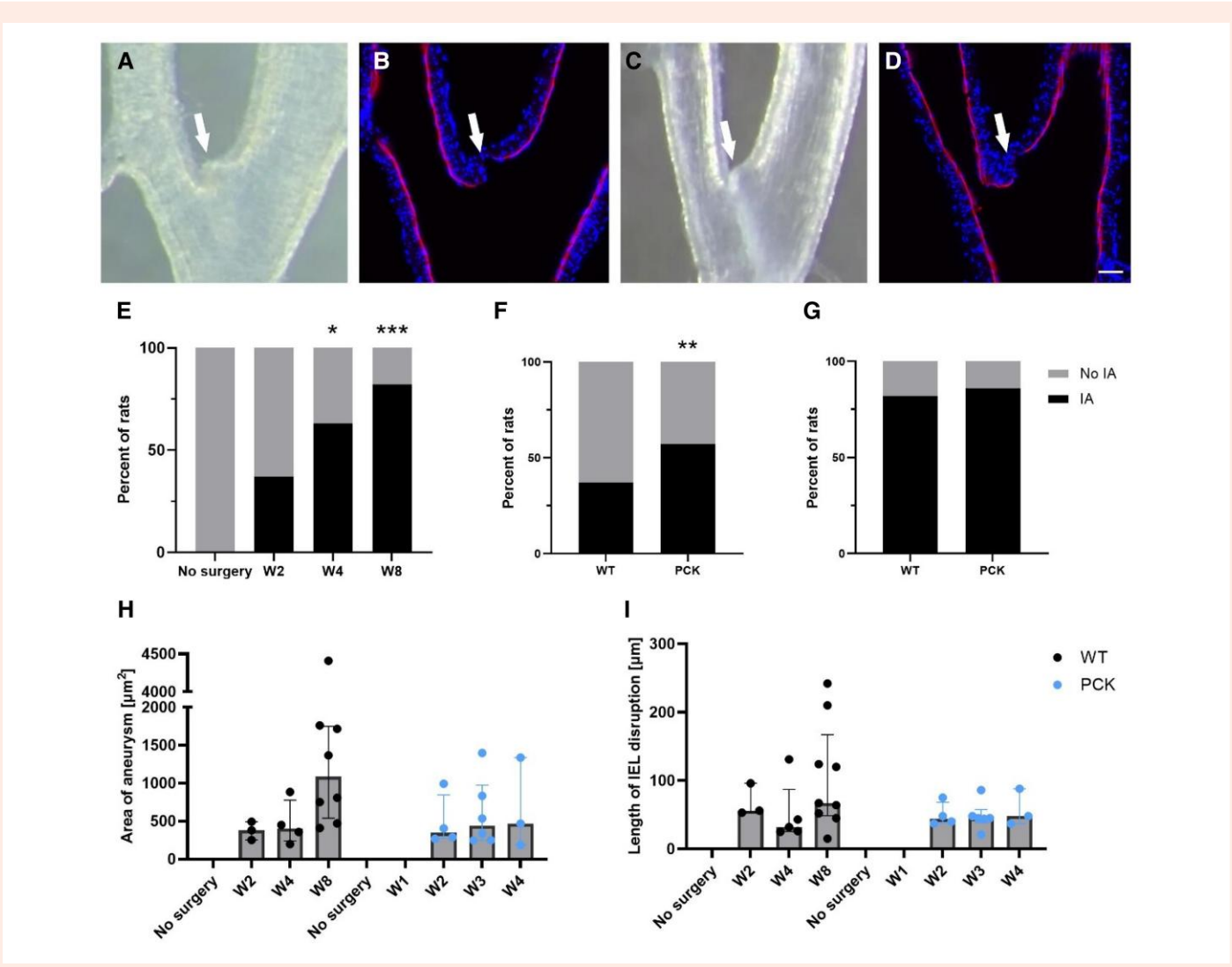

Figure 3 Faster IA development in PCK rats. (*A–D*) Representative images of IAs (white arrow) in a WT rat killed 8 weeks post-surgery (*A* and *B*) and a PCK rat killed 4 weeks post-surgery (*C* and *D*) observed under the dissection microscope (*A* and *C*) and sectioned and stained with DAPI (nuclei in blue) and Evans blue (elastic lamina in red) (*B* and *D*). Scale bar, 50 µm. (*E*) Quantification of IA development in WT rats over the 8 weeks experiment ($n = 8$–11/group). Fisher's exact test with controls without surgery. (*F*) Comparison of IA development between 8 WT and 7 PCK rats 2 weeks post-surgery. Fisher's exact test. (*G*) Comparison of IA development between 11 WT rats killed at 8 weeks post-surgery and 7 PCK rats killed at 3 weeks post-surgery. Fisher's exact test. *$P < 0.05$, **$P < 0.01$, ***$P < 0.001$. (*H* and *I*) Area of aneurysm (*H*) and length of internal elastic lamina disruption (*I*) at the level of the right OA-ACA bifurcation of WT ($n = 4$–11/group) and PCK rats ($n = 3$–6/group) killed without surgery or at 2–8 weeks post-surgery. Only rats with IAs were considered in (*H* and *I*). Kruskal–Wallis test with Dunn's multiple comparison test.

junctional proteins in IAs at the OA-ACA bifurcation and along the ACA, a region free of IA development, in control groups of WT and PCK rats and at 2 and 4 weeks post-surgery (*Figure 5A–D*). Importantly, staining for the endothelial marker CD31 was similar in all groups of WT and PCK rats both at the level of the ACA and OA-ACA bifurcation (*Figures 5B, E* and *F*), illustrating that the presence of endothelium was similar at both locations and not affected by the surgical procedure in rats with and without functional primary cilia. Next, we focused more specifically on the expression of the tight junction proteins ZO-1 (*Figure 5C*) and CLDN5 (*Figure 5D*) in the endothelium. At the level of the ACA, a similar increase of ZO-1 staining was observed 2 and 4 weeks post-surgery in ECs from WT ($P = 0.0123$ and $P = 0.0249$) and PCK rats ($P = 0.0003$ and $P = 0.0391$) in comparison to WT and PCK rats without surgery (*Figure 5G*). At the level of the IA, the ZO-1 staining was greatly increased in WT rats 2 weeks post-surgery ($P = 0.0200$) whereas this increase was absent in PCK rats (*Figure 5H*). Likewise, CLDN5 was increased in the OA-ACA bifurcation of WT rats ($P = 0.0067$ and $P = 0.0033$), and not of PCK rats, at 2 and 4 weeks post-surgery (*Figure 5J*).

Immunostainings on a limited number of PKD samples in our IA biobank showed reduced expression of ZO-1 in ECs of IA domes from PKD patients.[21] To investigate if the expression of ZO-1 and CLDN5 could serve as a marker for vulnerable IAs, the same endothelial tight junction proteins were studied in 19 vulnerable (ruptured) and 38 more stable (unruptured) human IA domes. Clinical data from patients with ruptured and unruptured IAs were not different (*Table 2*). As expected, maximal IA diameter and bottleneck factor were larger in ruptured IAs compared to unruptured IAs. Alike the rat IAs, ZO-1 immunostaining was lower in ruptured IAs compared to unruptured IAs ($P = 0.0373$) (*Figure 6A–C*). A similar decrease was observed for CLDN5 in ruptured IAs ($P = 0.0338$) (*Figure 6D–F*), while no difference in CD31 staining was observed between ruptured and unruptured IAs (*Figure 6G–I*). The decrease of tight junction proteins observed in IAs from PCK rats and in vulnerable human IAs might explain why IA in PKD patients at more at risk to rupture.

Downloaded from https://academic.oup.com/cardiovascres/advance-article/doi/10.1093/cvr/cvaf063/8115994 by guest on 21 May 2025

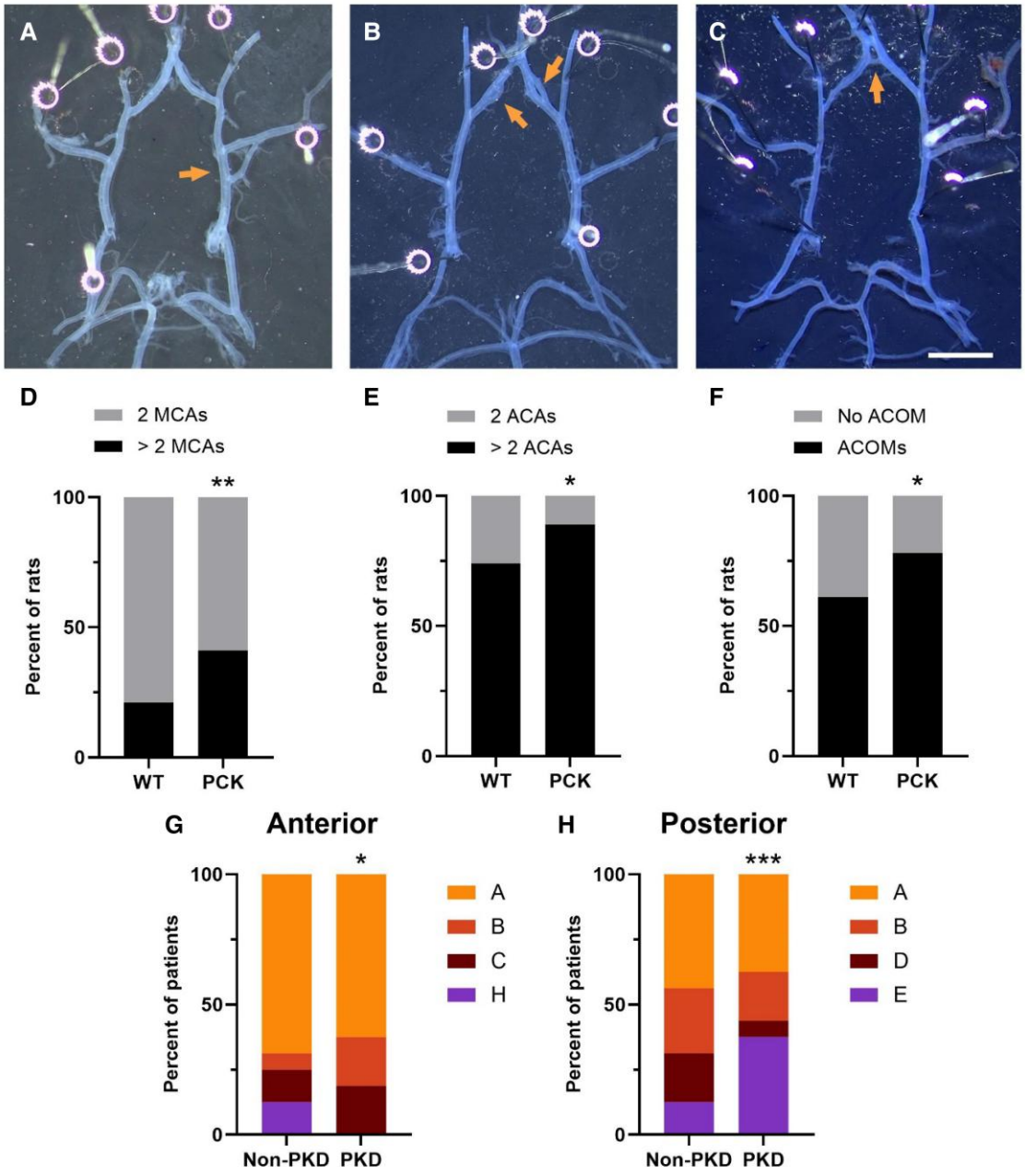

Figure 4 More variation in circle of Willis of PCK rats and PKD patients. (*A–C*) Representative images of three variations in the CoW observed in WT and PCK rats (arrows): additional MCA bifurcation (*A*), additional ACA bifurcation (*B*) and presence of an ACOM (*C*). Scale bar, 2 mm. MCA, middle cerebral artery. ACA, anterior cerebral artery. ACOM, anterior communicating artery. (*D–F*) Corresponding quantifications of these three CoW variations in WT ($n = 38$) and PCK ($n = 46$) rats. Fisher's exact test. (*G* and *H*) Prevalence of anterior (*G*) and posterior (*H*) variants of the CoW of PKD ($n = 16$) and matched non-PKD ($n = 16$) patients. Anatomic variations of the anterior and posterior part of the CoW are presented in Supplementary material online, *Figure S1*. Variants A are the normal configuration of the CoW. Anatomic variants of the anterior part: Variant B: Additional ACOM(s). Variant C: The median artery of the corpus callosum originates from the ACOM. Variant H: Hypoplasia or absence of the A1 segment of one of the ACAs. Anatomic variants of the posterior part: Variant B: One PCA originates predominantly from the ICA. This variation is also known as unilateral foetal type PCA. Variant D: Hypoplasia or absence of one PCOM. Variant E: Hypoplasia or absence of both PCOMs. Fisher's exact test. *$P < 0.05$, **$P < 0.01$ and ***$P < 0.001$.

3.6 Different IA wall remodelling in PCK rats

As a surrogate for vulnerability, we investigated CD68 positive macrophages (*Figure 7A* and *B*), known to secrete matrix metalloproteinases (MMPs) breaking down extracellular matrix, as well as Type I and Type III collagen (*Figure 7C*) during IA development in WT and PCK rats. At 2 weeks post-surgery, the number of CD68 positive cells was slightly increased in WT rats along the ACA, a region free of IA development ($P = 0.0309$) (*Figure 7D*) and in IAs at the OA-ACA bifurcation ($P = 0.0107$) (*Figure 7E*). A similar trend was observed for PCK rats. Importantly, no differences were observed between WT and PCK rats at similar time points, indicating that the inflammatory response during IA development was comparable in WT and PCK rats. Staining for Type

Downloaded from https://academic.oup.com/cardiovascres/advance-article/doi/10.1093/cvr/cvaf063/8115994 by guest on 21 May 2025

Table 1 Clinical data of the PKD and non-PKD patients

	ADPKD patients	Non-PKD patients	*P*-value
Patients	*n* = 16	*n* = 16	
Age, year: mean (SD)	55 (16)	64 (13)	0.09
Sex, female: *n* (%)	10 (63)	13 (81)	0.43
Multiple IAs: *n* (%)	8 (50)	7 (44)	>0.99
Previous aSAH: *n* (%)	0 (0)	0 (0)	>0.99
Positive family history for IA: *n* (%)	5 (31)	3 (19)	0.69
Smoker (former and current): *n* (%)	9 (56)	8 (50)	>0.99
Hypertension: *n* (%)	12 (75)	8 (50)	0.27

Comparison of means have been performed using two-tailed Student's *t*-test. Comparison of distribution have been performed using Fisher's exact test.
SD, standard deviation; aSAH, aneurysmal subarachnoid haemorrhage; IA, intracranial aneurysm.

I collagen was variable and not different in all groups of WT and PCK rats, both at the level of the ACA and OA-ACA bifurcation (*Figure 7F* and *G*). Staining for Type III collagen was similar in all groups of WT and PCK rats at the level of the ACA (*Figure 7H*) and in all groups of WT rats in IAs at the OA-ACA bifurcation (*Figure 7I*). Interestingly, the content of Type III collagen tended to decrease with time post-surgery in PCK rats and was considerably lower in IAs of PCK rats compared to WT rats at 4 weeks post-surgery ($P = 0.0141$) (*Figure 7I*), highlighting a different collagen remodelling during IA development in PCK rats compared to WT rats.

4. Discussion

The mechanisms leading to increased risk for PKD patients to develop more IAs of increased vulnerability are still not completely understood. In this study, we used young PCK rats that have a similar weight curve than WT rats (until maximal 14 weeks of age) but develop cysts in the kidneys already at 21 days of age.[25] Despite the presence of cysts in the kidneys, PCK rats did not develop a higher BP than WT rats following the protocol to induce IAs (*Figure 1*). This protocol however drastically increased the mortality of PCK rats after 3 weeks post-surgery. We uncovered that aortic dissection causing fatal thoracic haemorrhage was the cause of death (*Figure 2*). Interestingly, IAs developed faster in PCK rats compared to WT rats (*Figure 3*), suggesting that PCK rats are more sensitive to IA induction. In addition, we observed an increased frequency of anatomical variations in the CoW of PCK rats and PKD patients compared to WT rats and non-PKD patients (*Figure 4*). The increased expression of tight junction proteins observed in WT rats after IA induction was not observed in PCK rats (*Figure 5*). A similar decrease in tight junction protein expression was observed in vulnerable (ruptured) IAs compared to more stable (unruptured) IAs (*Figure 6*). Finally, a lower content of Type III collagen pointed to a different IA wall remodelling in PCK rats compared to WT rats (*Figure 7*). Thus, variations in the anatomy of the CoW and impaired regulation of tight junction proteins might put PCK rats and PKD patients more at risk to develop vulnerable IAs.

The PKD patients included in the @neurIST study are all ADPKD patients, as ARPKD is an infantile form of PKD associated with shortened life expectancy. The autosomal dominant and recessive forms of PKD are both associated with a lack of functional primary cilia[20] and an increased frequency of IAs.[12,14,19] However, the primary cilia are differentially affected in ADPKD and ARPKD, as the various forms affect different proteins, i.e. the polycystin-1, polycystin-2, or fibrocystin/polyductin protein, respectively. Similar to ARPKD patients,[30] primary cilia in PCK rats were shown to exhibit various abnormalities,[26,31] while primary cilia in ADPKD patients present rather a dysfunction than structural abnormalities.[20,32] Despite these differences in ADPKD patients and PCK rats, both characterized by a lack of functional primary cilia, we observed several similarities in the present and previous study from our group,[21] i.e. a similar decrease in tight junction proteins, a lower Type III collagen content and an increased frequency of anatomical variations in the CoW in both PCK rats and ADPKD patients.

The protocol to induce IAs unexpectedly increased the mortality of PCK rats. It has been previously described that PKD signs affect PCK rats and decrease their survival after 17 weeks of age.[33] In our experiment, we observed a decreased survival at 3 weeks post-surgery, which corresponds to 9- to 13-week-old rats. It is thus unlikely that the premature death of PCK animals in our study resulted directly from PKD, and we assume that the aortic dissection resulting in the premature death of PCK rats is a consequence of the IA induction protocol. Of further note, the increased frequency of aortic dissection is also unlikely to be a direct consequence of PKD-induced hypertension since we observed similar levels of hypertension in WT and PCK rats. Indeed, the PCK rats used in this study were a maximum of 13 weeks old, and PKD has not progressed enough to affect systolic BP at this young age.[34,35] Angiolathyrism induced by the lathyritic compound BAPN, which inhibits the cross-linking between elastin and collagen,[36] facilitates IA development in combination with increased haemodynamic stress and hypertension in this IA rat model.[37] BAPN affects not only intracranial arteries, but all blood vessels and thoracic haemorrhage has been described by Hashimoto and colleagues[38] in WT rats exposed to the IA induction protocol. In this study, however, BAPN was described to mostly affect young and growing animals and to have less effect in adult WT rats. Our study revealed severe alterations in the elastic architecture of the aortic wall in adult PCK rats at 4 weeks post-surgery, to which BAPN certainly contributed. Pulsatile cardiac outflow at high pressure might be an additional damaging factor given the observed more severe morphological alterations in the ascending aorta. It is noteworthy that PKD patients are not only at higher risk of IA development but also display an increased risk of developing aortic aneurysms and dissections.[39,40] Altogether, we postulate that the lack of functional primary cilia in the endothelium of PCK rats in combination with the induced hypertension and the BAPN treatment drastically increased the risk of developing aortic dissection in the PCK rats through an alteration of the elastic architecture.

A majority of the population lacks a full CoW[41] and variations in the CoW have been correlated with IA disease.[10,11] Moreover, the CoW of women, who are at greater risk to develop IAs, was shown to be different from men and the distribution of IA locations was also shown to be different.[42,43] In our study, we observed more anatomical variation in the CoW of PKD patients and PCK rats than in the CoW of non-PKD patients and WT rats. Furthermore, a recent meta-analysis onto IA distribution in patients with ADPKD revealed different IA locations in this subgroup than in the general population.[44] Indeed, PKD patients developed more often IAs in large diameter arteries like MCA, ICA, and ACOM.[44] As a different organization modifies the blood flow pattern within the CoW, the different IA locations in PKD patients might be due to their different CoW organization, as suggested by the results of this study. The embryonic development of the CoW is greatly influenced by genetic factors.[41,45] Moreover, the development of the vascular system during embryogenesis is highly regulated by blood flow.[46] Therefore, lack of functional primary cilia in ECs of PKD patients might impact the arterial growth and branching during embryogenesis leading to a different CoW organization. Subsequently, the variation in haemodynamics resulting from this different CoW organization explains the increased risk to develop IAs. In addition, variability of the CoW configuration has been associated with an increased risk of IA rupture.[47,48] Thus, screening for anatomical variations in the CoW might help to identify non-PKD patients that are at greater risk of IA rupture and may further open the way to personalized decisions for IA treatment.

In accordance with an earlier study in different mouse models of PKD,[49] we found that IAs developed faster in PCK rats compared to WT rats. As this rat and the mouse PKD model carry different mutations, this strongly suggests a causal relation between the absence of functional endothelial primary cilia and the sensitivity to develop IAs. As previously demonstrated

Downloaded from https://academic.oup.com/cardiovascres/advance-article/doi/10.1093/cvr/cvaf063/8115994 by guest on 21 May 2025

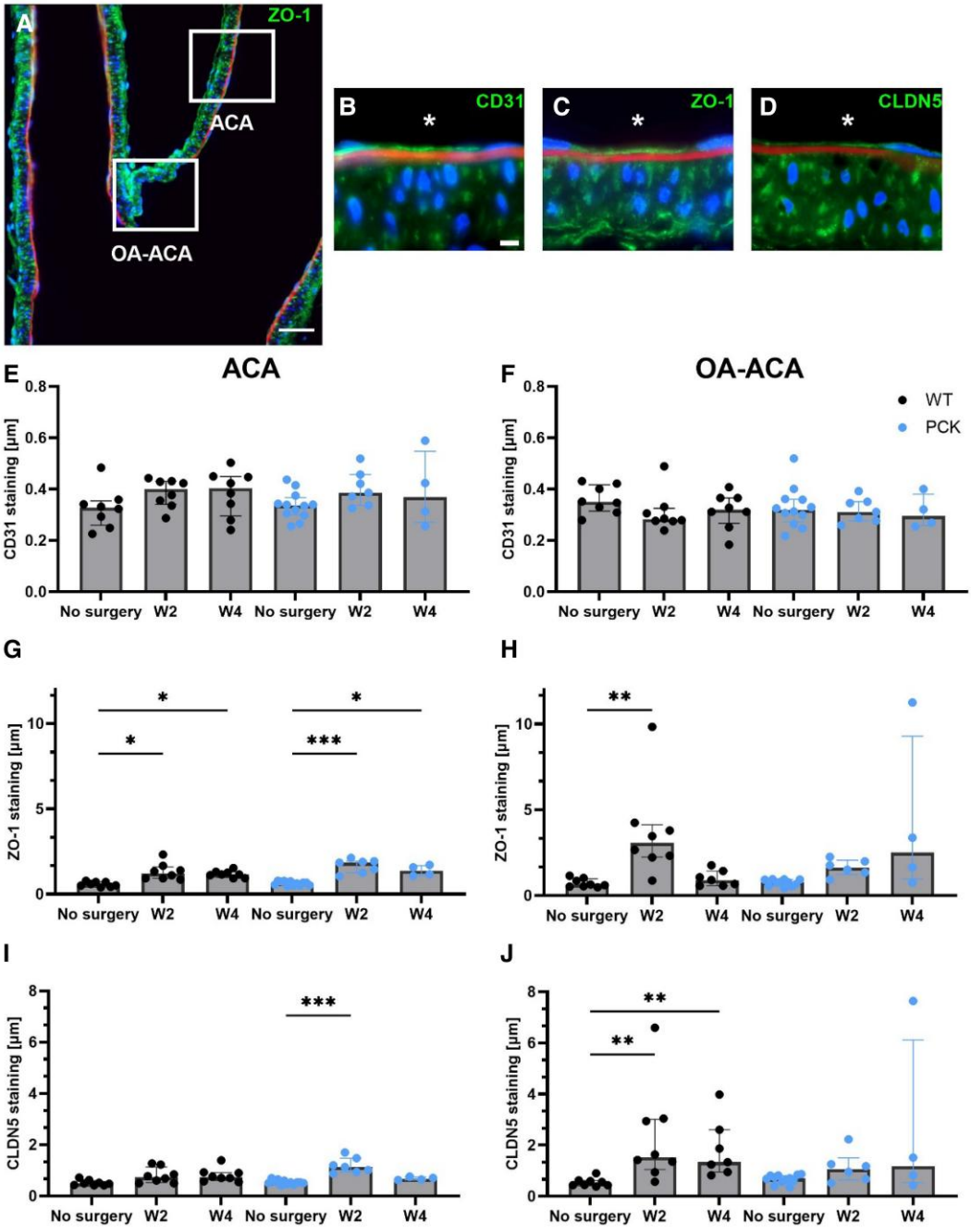

Figure 5 Absence of increase in endothelial tight junction proteins in IAs of PCK rats. (*A*) Representative ZO-1 immunostaining of the right OA-ACA bifurcation of a WT rat killed 8 weeks post-surgery. The white squares indicate two zones of interest: the OA-ACA bifurcation where IAs develop and a straight part of the ACA. Scale bar, 50 µm. (*B–D*) Representative CD31 (*B*), ZO-1 (*C*) and CLDN5 (*D*) immunostainings (in green). Nuclei are stained with DAPI (in blue), and internal elastic laminae are stained with Evans blue (in red). * denotes lumen of the vessel. Scale bar, 5 µm. (*E–J*), Quantifications of CD31 (*E* and *F*), ZO-1 (*G* and *H*) and CLDN5 (*I* and *J*) immunostainings on WT ($n = 7–8$/group) and PCK ($n = 4–11$/group) rats killed without surgery, at 2 and 4 weeks post-surgery in the ACA (*E*, *G*, and *I*) and at the OA-ACA bifurcation (*F*, *H* and *J*). Kruskal–Wallis test with Dunn's multiple comparison test with WT and PCK without surgery. *$P < 0.05$, **$P < 0.01$, ***$P < 0.001$.

in vitro, primary cilia dampen the endothelial response to an aneurysmal pattern of disturbed flow.[21] Thus, an exaggerated endothelial response to disturbed blood flow may cause more IAs in PKD patients. Interestingly, PKD patients have not only an increased sensitivity to IA development but they are also classified as a high risk group for aneurysmal SAH,[50] suggesting that their IA are more susceptible to rupture.

We previously observed a reduction of the tight junction protein ZO-1 in the endothelium of IA domes from PKD patients in comparison to non-PKD patients.[21] As ZO-1 is crucial for an intact endothelial barrier, we postulated that a decrease of ZO-1 might explain why IAs of PKD patients are more at risk of rupture. To investigate a possible causal relation between the absence of functional endothelial primary cilia and IA

Downloaded from https://academic.oup.com/cardiovascres/advance-article/doi/10.1093/cvr/cvaf063/8115994 by guest on 21 May 2025

Table 2 Patient and IA characteristics of patients with ruptured and unruptured IAs

	Ruptured IAs	Unruptured IAs	*P*-value
Patients	***n* = 19**	***n* = 38**	
Age, year: mean (SD)	51 (11)	56 (11)	0.14
Sex, female: *n* (%)	14 (74)	27 (71)	>0.99
Multiple IAs: *n* (%)	8 (44) ▲	20 (53)	0.78
Previous aSAH: *n* (%)	2 (11) ▲	5 (13)	>0.99
Positive family history for IA: *n* (%)	2 (11) ▲	5 (14) ▲	>0.99
Smoker (former and current): *n* (%)	12 (67) ▲	28 (74)	0.75
Hypertension: *n* (%)	6 (33) ▲	14 (37)	>0.99
Intracranial aneurysm	***n* = 19**	***n* = 38**	
Rough appearance: *n* (%)	5 (33) ▼	17 (46) ▲	0.54
Presence of blebs or lobules: *n* (%)	13 (72) ▲	20 (53)	0.25
Neck size, mm: median (IQR)	3.6 (2.6–4.9) ►	3.8 (3.0–5.0)	0.79
Maximal diameter, mm: median (IQR)	7.9 (5.8–10.6) ▲	5.7 (4.2–8.2)	0.03
Bottleneck factor: median (IQR)	2.0 (1.4–2.7) ►	1.6 (1.2–1.8)	0.03

Comparison of means and medians have been performed using two-tailed Student's *t*-test and Mann–Whitney *U*-test, respectively. Comparison of distribution have been performed using Fisher's exact test. Missing information for 1 (▲), 3 (►), or 4 (▼) patients.
SD, standard deviation; IQR, interquartile range. aSAH, aneurysmal subarachnoid haemorrhage; IA, intracranial aneurysm.

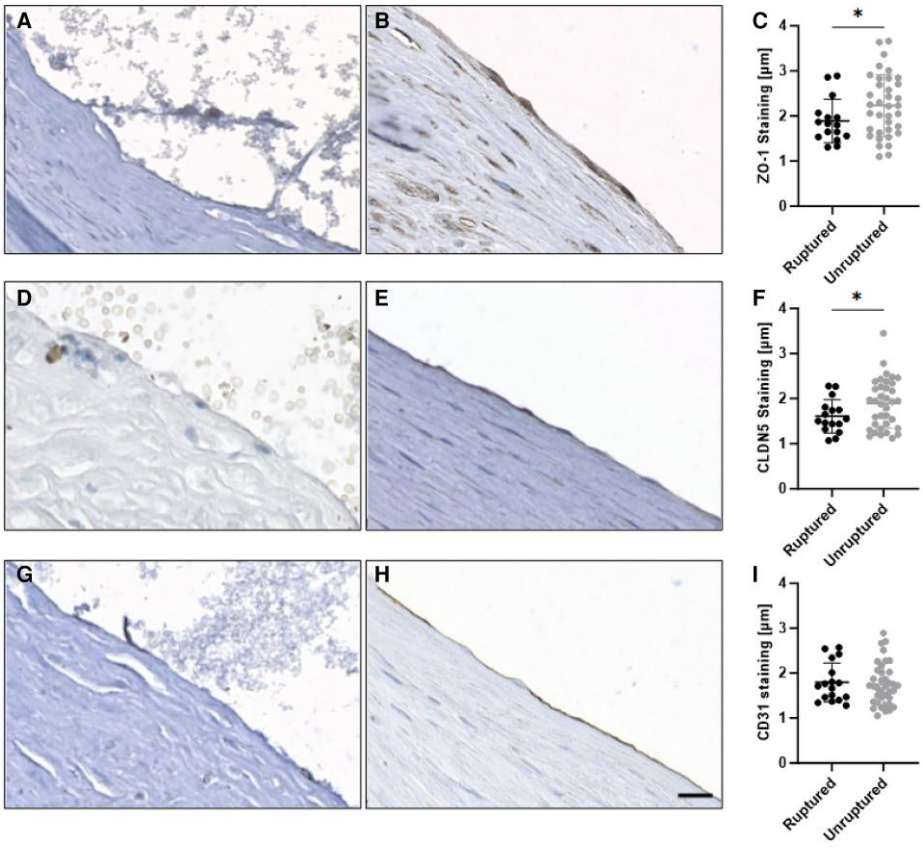

Figure 6 Decreased endothelial tight junction proteins in ruptured IAs of patients. (*A–C*) ZO-1 immunostaining (in brown) on ruptured (*A*) and unruptured (*B*) human IAs and corresponding quantification (*C*) on ruptured ($n = 16$) and unruptured ($n = 36$) IAs. (*D–F*) CLDN5 immunostaining (in brown) on ruptured (*D*) and unruptured (*E*) human IAs and corresponding quantification (*F*) on ruptured ($n = 16$) and unruptured ($n = 36$) IAs. (*G–I*) CD31 immunostaining (in brown) on ruptured (*G*) and unruptured (*H*) human IAs and corresponding quantification (*I*) on ruptured ($n = 17$) and unruptured ($n = 38$) IAs. One-tailed Student's *t*-tests were conducted, as a lower expression of tight junction proteins in vulnerable IAs was expected based on previous results.[21] Using two-tailed Student's *t*-tests would have doubled the *P*-values (i.e. 0.0746 for ZO-1 and 0.0675 for CLND5). Scale bar, 20 µm. $*P < 0.05$.

Downloaded from https://academic.oup.com/cardiovascres/advance-article/doi/10.1093/cvr/cvaf063/8115994 by guest on 21 May 2025

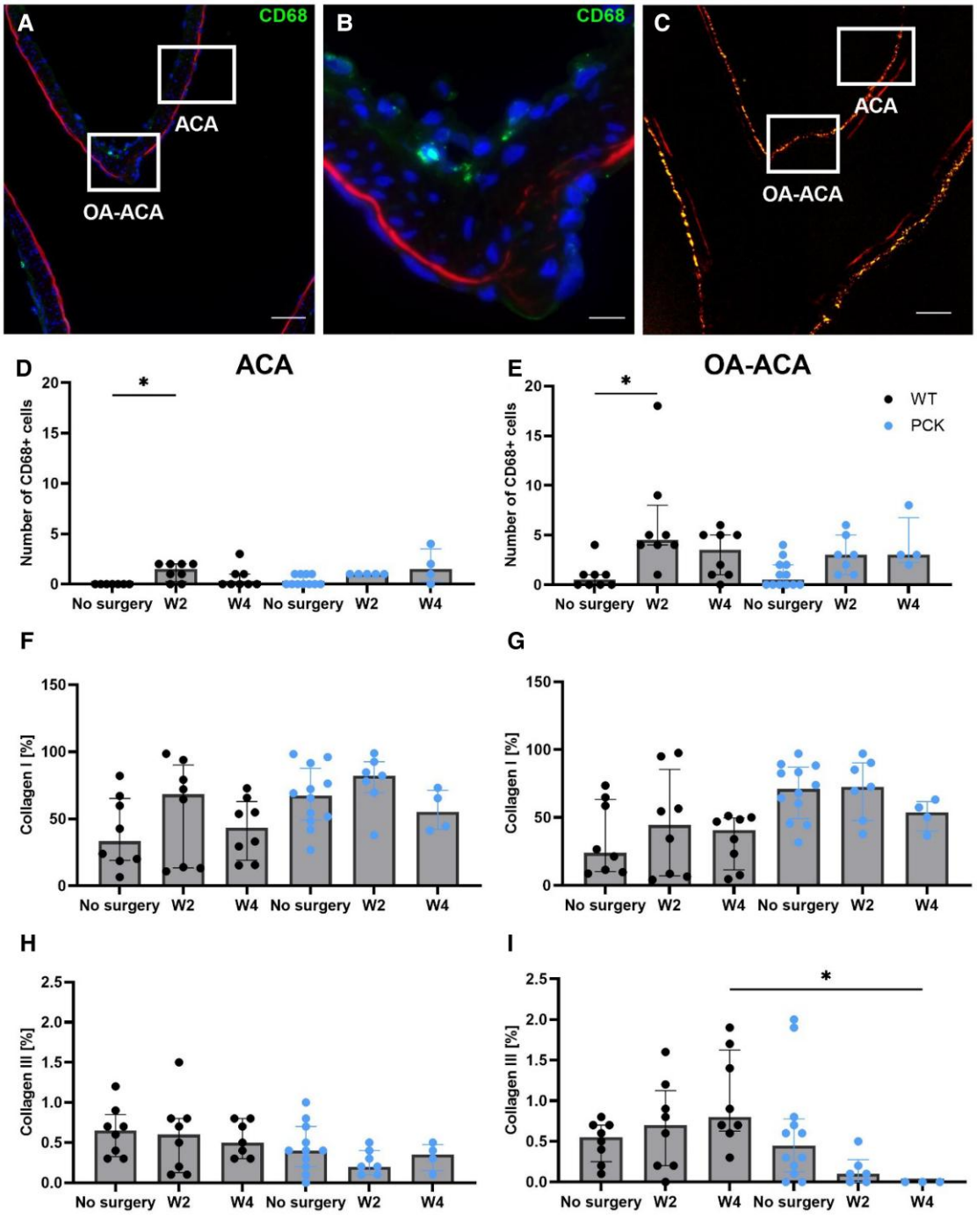

Figure 7 Different IA wall remodelling in PCK rats. (*A* and *B*) Representative CD68 immunostaining (in green) of the right OA-ACA bifurcation of a WT rat killed 8 weeks post-surgery. The white squares indicate two zones of interest: the OA-ACA bifurcation where IAs develop and a straight part of the ACA. (*B*) is a magnification of (*A*) showing infiltration of CD68 positive cells in IA wall. Scale bar, 50 μm in (*A*) and 10 μm in (*B*). Nuclei are stained with DAPI (in blue), and internal elastic laminae are stained with Evans blue (in red). (*C*) Representative picrosirius red staining of the right OA-ACA bifurcation of a WT rat killed 8 weeks post-surgery, visualized by polarized light. Type I collagen is stained in yellow-red and Type III collagen is stained in green. Scale bar, 50 μm. Quantification of the number of CD68 positive cells (*D* and *E*), percentage of Type I collagen (*F* and *G*) and Type III collagen (*H* and *I*) on WT ($n = 7$–8/group) and PCK ($n = 3$–12/group) rats killed without surgery, at 2 and 4 weeks post-surgery in the ACA (*D*, *F*, and *H*) and at the OA-ACA bifurcation (*E*, *G*, and *I*). Kruskal–Wallis test with Dunn's multiple comparison test with WT vs. PCK without surgery and WT and PCK at similar timepoint. $*P < 0.05$.

vulnerability, we investigated PCK rats and studied the expression of the tight junction proteins ZO-1 and CLDN5 in the endothelium of IAs at the OA-ACA bifurcation, a preference location of primary cilia,[21] and in the endothelium of a non-IA region of the ACA. ECs in WT and PCK rats showed a similar increase in ZO-1 and CLDN5 staining at the level of the ACA 2 and 4 weeks post-surgery, which is likely an adaptive response

Downloaded from https://academic.oup.com/cardiovascres/advance-article/doi/10.1093/cvr/cvaf063/8115994 by guest on 21 May 2025

to the increased haemodynamic stress and hypertension. The molecular mechanism responsible for this adaptive response was not studied. However, it is known that endothelial tight junction protein expression can be regulated through the Akt1-FoxO signalling pathway[51] or the Angiopoietin-Tie signalling pathway.[52] Interestingly, at the level of the OA-ACA bifurcation, where IAs develop, the adaptive increase in ZO-1 and CLDN5 staining was only observed in WT rats. The absence of this protective effect at the OA-ACA bifurcation might be a further explanation as to why IAs develop faster in PCK rats. The lack of an adaptive tight junction-strengthening response in PCK rats may also facilitate macrophage infiltration over the endothelial barrier into the IA as postulated by Tada *et al.*[53] thereby enhancing inflammation, collagen degradation and vulnerability of the IA. Although the number of CD68 positive macrophages was similar in WT and PCK IA development, a different collagen remodelling was observed in IA walls from PCK rats. Extracellular matrix remodelling is a dynamic process involving both the synthesis and degradation of collagen in response to mechanical stress and biochemical stimuli.[54] In our study, at 4 weeks post-surgery, the content of Type III collagen was lower in IA walls of PCK rats compared to WT rats. These findings align with our previous investigations of IA walls in PKD patients, which revealed no differences in macrophage content but noted differences in collagen content between IAs from PKD and non-PKD patients.[21] Collagen plays a crucial role in maintaining the integrity of the IA wall, as it provides tensile strength and elasticity necessary to resist aneurysm growth and rupture. A reduction in Type III collagen could compromise the wall's load-bearing capacity, increasing its susceptibility to rupture.[54] Different collagen remodelling processes, such as reduced collagen production by smooth muscle cells and fibroblasts, or increased collagen breakdown by MMPs might explain the lower Type III collagen content in IA wall observed in our study. Macrophages secrete MMPs that degrade collagens. Intriguingly, increased levels of MMP-2 and MMP-9 were found in patients with acute aortic dissection at the sites of intimal tears.[55] Moreover, using the same rat IA model, Aoki *et al.*[56] observed that aneurysm growth was closely associated with MMP-2 and MMP-9 expression and that inhibition of these MMPs prevented IA progression. Since the number of macrophages was not different in our study while Type III collagen was lower in IAs of PCK rats and PKD patients, it would be interesting to investigate if lack of functional primary cilia would affect the MMPs secretion by macrophages. Such experiments are however beyond the scope of this study.

Several groups have found that vulnerable (i.e. ruptured) IA walls contain more CD68 positive cells and have a lower collagen content than stable (i.e. unruptured) IA walls.[29,57–59] In a previous study, we observed a lower content of Type I and Type III collagens in ruptured IA walls compared to unruptured IA walls.[29] Thus, the lower content of Type III collagen observed in IA walls from PCK rats and PKD patients might weaken the IA wall and explain (in part) the higher risk of IA rupture in PKD patients.

Finally, it should be noted that while using the Aoki IA induction protocol on PCK rats provided much new (mechanistic) information, it has certain limitations due to differences from human PKD. For instance, the progression and severity of cyst formation in PCK rats differ from those observed in PKD patients.[60] Thus, PCK rats may be more susceptible to aspects of the protocol used to induce IAs, which might not fully reflect the factors influencing IA development in PKD patients. Another limitation of our study is that IA development could only be studied for a relatively short period of time (3–4 weeks) in PCK rats. Moreover, the high mortality of PCK rats might have introduced a bias as we could only study the surviving rats. In addition, the IA induction protocol used in this study gives rise to stable IAs with a very low rupture rate in WT rats.[61] Although IAs in PCK rats seemed to have a more vulnerable phenotype based on tight junction protein expression, our study did not investigate IA rupture and can thus only postulate towards the increased risk of IA rupture in PKD patients. Other IA animal models exist to study IA rupture,[62,63] but PCK rats might be too sensitive to such protocols given the drastic decrease in survival following the present IA induction protocol. We recognize that sex is an important variable in animal studies and clinical presentation of disease. A limitation of our study is that it has been performed in male rats only.[64] Finally, the protocol used to induce IAs in rats resulted in the formation of small IAs, which limits the amount of study material and thus the extent to which conclusions drawn from IAs in PCK rats can be applied to those in PKD patients.

In conclusion, PCK rats are more vulnerable to IA induction and developed IAs faster than WT rats. IA development is a complex process influenced by several factors. We observed variations in the CoW anatomy and an impaired regulation of tight junction proteins in PCK rats which might explain the increased incidence of IAs in PKD patients. Moreover, these differences as well as the lower Type III collagen content may also explain why PKD patients are more at risk of IA rupture. Finally, these differences might help to identify non-PKD patients who are at greater risk of IA rupture.

Translational perspective

Polycystic kidney disease (PKD) is associated with a high intracranial aneurysm (IA) incidence and risk of rupture. PKD patients carry a gene mutation affecting primary cilia, blood flow mechano-sensors in endothelial cells. Here, we found that IAs developed faster in a PKD rat model than in wild-type rats, which was likely due to the combination of impaired regulation of tight junction proteins and increased anatomical variations in the circle of Willis. These findings explain the higher incidence and rupture risk of IAs in PKD patients and may also help to identify non-PKD patients at greater risk of IA rupture.

Supplementary material

Supplementary material is available at *Cardiovascular Research* online.

Acknowledgements

The authors thank Bernard Foglia, Graziano Pelli, Marc Saulnier-Navetier, Fadi Haidar, and Abiram Sandralegar for technical assistance and helpful discussions. Collection of clinical data and images have been performed with the help of the HUG NeuroCentre, Geneva University Hospitals, Geneva, Switzerland.

Conflict of interest: None declared.

Funding

This work was supported by the Fondation Privée des Hôpitaux Universitaires de Genève (grant number RC05-02 to B.R.K., E.A., and P.B.), the Gottfried und Julia Bangerter-Rhyner-Stiftung (to B.R.K.), the Wolfermann-Nägeli-Stiftung (to B.R.K.), the Swiss Heart Foundation (grant number FF22011 to B.R.K., E.A., and P.B.), and the Swiss National Science Foundation (grant number 320030-231430 to B.R.K., E.A., and P.B.).

Data availability

The data underlying this article will be shared on reasonable request to the corresponding author.

Downloaded from https://academic.oup.com/cardiovascres/advance-article/doi/10.1093/cvr/cvaf063/8115994 by guest on 21 May 2025

References

1. Brisman JL, Song JK, Newell DW. Cerebral aneurysms. *N Engl J Med* 2006;**355**:928–939.
2. Texakalidis P, Sweid A, Mouchtouris N, Peterson EC, Sioka C, Rangel-Castilla L, Reavey-Cantwell J, Jabbour P. Aneurysm formation, growth, and rupture: the biology and physics of cerebral aneurysms. *World Neurosurg* 2019;**130**:277–284.
3. Lawton MT, Vates GE. Subarachnoid hemorrhage. *N Engl J Med* 2017;**377**:257–266.
4. Darsaut TE, Findlay JM, Magro E, Kotowski M, Roy D, Weill A, Bojanowski MW, Chaalala C, Iancu D, Lesiuk H, Sinclair J, Scholtes F, Martin D, Chow MM, O'Kelly CJ, Wong JH, Butcher K, Fox AJ, Arthur AS, Guilbert F, Tian L, Chagnon M, Nolet S, Gevry G, Raymond J. Surgical clipping or endovascular coiling for unruptured intracranial aneurysms: a pragmatic randomised trial. *J Neurol Neurosurg Psychiatry* 2017;**88**:663–668.
5. Diagbouga MR, Morel S, Bijlenga P, Kwak BR. Role of hemodynamics in initiation/growth of intracranial aneurysms. *Eur J Clin Invest* 2018;**48**:e12992.
6. Kapoor K, Kak VK, Singh B. Morphology and comparative anatomy of circulus arteriosus cerebri in mammals. *Anat Histol Embryol* 2003;**32**:347–355.
7. Kızılgöz V, Kantarcı M, Kahraman Ş. Evaluation of circle of Willis variants using magnetic resonance angiography. *Sci Rep* 2022;**12**:17611.
8. Krabbe-Hartkamp MJ, van der Grond J, de Leeuw FE, de Groot JC, Algra A, Hillen B, Breteler MM, Mali WP. Circle of Willis: morphologic variation on three-dimensional time-of-flight MR angiograms. *Radiology* 1998;**207**:103–111.
9. Alnaes MS, Isaksen J, Mardal KA, Romner B, Morgan MK, Ingebrigtsen T. Computation of hemodynamics in the circle of Willis. *Stroke* 2007;**38**:2500–2505.
10. Kayembe KN, Sasahara M, Hazama F. Cerebral aneurysms and variations in the circle of Willis. *Stroke* 1984;**15**:846–850.
11. Krasny A, Nensa F, Sandalcioglu IE, Göricke SL, Wanke I, Gramsch C, Sirin S, Oezkan N, Sure U, Schlamann M. Association of aneurysms and variation of the A1 segment. *J Neurointerv Surg* 2014;**6**:178–183.
12. Cornec-Le Gall E, Alam A, Perrone RD. Autosomal dominant polycystic kidney disease. *Lancet* 2019;**393**:919–935.
13. Bergmann C, Guay-Woodford LM, Harris PC, Horie S, Peters DJM, Torres VE. Polycystic kidney disease. *Nat Rev Dis Primers* 2018;**4**:50.
14. Kuo IY, Chapman A. Intracranial aneurysms in ADPKD: how far have we come? *Clin J Am Soc Nephrol* 2019;**14**:1119–1121.
15. De Blasi R, Lasjaunias P, Rodesch G, Alvarez H. Endovascular treatment of a ruptured intracranial arterial aneurysm in a 12-year-old child with recessive polycystic kidney disease. *Interv Neuroradiol* 1997;**3**:333–336.
16. Neumann HP, Krumme B, van Velthoven V, Orszagh M, Zerres K. Multiple intracranial aneurysms in a patient with autosomal recessive polycystic kidney disease. *Nephrol Dial Transplant* 1999;**14**:936–939.
17. Lilova MI, Petkov DL. Intracranial aneurysms in a child with autosomal recessive polycystic kidney disease. *Pediatr Nephrol* 2001;**16**:1030–1032.
18. Chalhoub V, Abi-Rafeh L, Hachem K, Ayoub E, Yazbeck P. Intracranial aneurysm and recessive polycystic kidney disease: the third reported case. *JAMA Neurol* 2013;**70**:114–116.
19. Perez JL, McDowell MM, Zussman B, Jadhav AP, Miyashita Y, McKiernan P, Greene S. Ruptured intracranial aneurysm in a patient with autosomal recessive polycystic kidney disease. *J Neurosurg Pediatr* 2019;**23**:75–79.
20. Ma M. Cilia and polycystic kidney disease. *Semin Cell Dev Biol* 2021;**110**:139–148.
21. Diagbouga MR, Morel S, Cayron AF, Haemmerli J, Georges M, Hierck BP, Allémann E, Lemeille S, Bijlenga P, Kwak BR. Primary cilia control endothelial permeability by regulating expression and location of junction proteins. *Cardiovasc Res* 2022;**118**:1583–1596.
22. Cong X, Kong W. Endothelial tight junctions and their regulatory signaling pathways in vascular homeostasis and disease. *Cell Signal* 2020;**66**:109485.
23. Greene C, Hanley N, Campbell M. Claudin-5: gatekeeper of neurological function. *Fluids Barriers CNS* 2019;**16**:3.
24. Lochhead JJ, Yang J, Ronaldson PT, Davis TP. Structure, function, and regulation of the blood-brain barrier tight junction in central nervous system disorders. *Front Physiol* 2020;**11**:914.
25. Lager DJ, Qian Q, Bengal RJ, Ishibashi M, Torres VE. The pck rat: a new model that resembles human autosomal dominant polycystic kidney and liver disease. *Kidney Int* 2001;**59**:126–136.
26. Mason SB, Liang Y, Sinders RM, Miller CA, Eggleston-Gulyas T, Crisler-Roberts R, Harris PC, Gattone VH II. Disease stage characterization of hepatorenal fibrocystic pathology in the PCK rat model of ARPKD. *Anat Rec (Hoboken)* 2010;**293**:1279–1288.
27. Aoki T, Nishimura M. The development and the use of experimental animal models to study the underlying mechanisms of CA formation. *J Biomed Biotechnol* 2011;**2011**:535921.
28. Aoki T, Frösen J, Fukuda M, Bando K, Shioi G, Tsuji K, Ollikainen E, Nozaki K, Laakkonen J, Narumiya S. Prostaglandin E2-EP2-NF-κB signaling in macrophages as a potential therapeutic target for intracranial aneurysms. *Sci Signal* 2017;**10**:eaah6037.
29. Morel S, Diagbouga MR, Dupuy N, Sutter E, Braunersreuther V, Pelli G, Corniola M, Gondar R, Jägersberg M, Isidor N, Schaller K, Bochaton-Piallat ML, Bijlenga P, Kwak BR. Correlating clinical risk factors and histological features in ruptured and unruptured human intracranial aneurysms: the Swiss AneuX Study. *J Neuropathol Exp Neurol* 2018;**77**:555–566.
30. Molinari E, Srivastava S, Dewhurst RM, Sayer JA. Use of patient derived urine renal epithelial cells to confirm pathogenicity of PKHD1 alleles. *BMC Nephrol* 2020;**21**:435.
31. Muff MA, Masyuk TV, Stroope AJ, Huang BQ, Splinter PL, Lee SO, Larusso NF. Development and characterization of a cholangiocyte cell line from the PCK rat, an animal model of autosomal recessive polycystic kidney disease. *Lab Invest* 2006;**86**:940–950.
32. Kathem SH, Mohieldin AM, Nauli SM. The roles of primary cilia in polycystic kidney disease. *AIMS Mol Sci* 2014;**1**:27–46.
33. Katsuyama M, Masuyama T, Komura I, Hibino T, Takahashi H. Characterization of a novel polycystic kidney rat model with accompanying polycystic liver. *Exp Anim* 2000;**49**:51–55.
34. Sato Y, Qiu J, Miura T, Kohzuki M, Ito O. Effects of long-term exercise on liver cyst in polycystic liver disease model rats. *Med Sci Sports Exerc* 2020;**52**:1272–1279.
35. Goto M, Hoxha N, Osman R, Dell KM. The renin-angiotensin system and hypertension in autosomal recessive polycystic kidney disease. *Pediatr Nephrol* 2010;**25**:2449–2457.
36. Barrow MV, Simpson CF, Miller EJ. Lathyrism: a review. *Q Rev Biol* 1974;**49**:101–128.
37. Suzuki S, Robertson JT, White RP, Stadlan EM, Popoff N. Experimental intracranial aneurysms in rats. A gross and microscopic study. *J Neurosurg* 1980;**52**:494–500.
38. Handa H, Hashimoto N, Nagata I, Hazama F. Saccular cerebral aneurysms in rats: a newly developed animal model of the disease. *Stroke* 1983;**14**:857–866.
39. Sung PH, Yang YH, Chiang HJ, Chiang JY, Chen CJ, Liu CT, Yu CM, Yip HK. Risk of aortic aneurysm and dissection in patients with autosomal-dominant polycystic kidney disease: a nationwide population-based cohort study. *Oncotarget* 2017;**8**:57594–57604.
40. Neves JB, Rodrigues FB, Lopes JA. Autosomal dominant polycystic kidney disease and coronary artery dissection or aneurysm: a systematic review. *Ren Fail* 2016;**38**:493–502.
41. Iqbal S. A comprehensive study of the anatomical variations of the circle of Willis in adult human brains. *J Clin Diagn Res* 2013;**7**:2423–2427.
42. Ophelders MEH, van Eldik MJA, Vos IN, Beentjes YS, Velthuis BK, Ruigrok YM. Anatomical differences of intracranial arteries according to sex: a systematic review and meta-analysis. *J Neuroradiol* 2024;**51**:10–15.
43. Horikoshi T, Akiyama I, Yamagata Z, Sugita M, Nukui H. Magnetic resonance angiographic evidence of sex-linked variations in the circle of willis and the occurrence of cerebral aneurysms. *J Neurosurg* 2002;**96**:697–703.
44. Haemmerli J, Morel S, Georges M, Haidar F, Chebib FT, Morita A, Nozaki K, Tominaga T, Bervitskiy AV, Rzaev J, Schaller K, Bijlenga P. Characteristics and distribution of intracranial aneurysms in patients with autosomal dominant polycystic kidney disease compared with the general population: a meta-analysis. *Kidney360* 2023;**4**:e466–e475.
45. Faber JE, Zhang H, Rzechorzek W, Dai KZ, Summers BT, Blazek C, Hedges SJ. Genetic and environmental contributions to variation in the posterior communicating collaterals of the circle of Willis. *Transl Stroke Res* 2019;**10**:189–203.
46. le Noble F, Fleury V, Pries A, Corvol P, Eichmann A, Reneman RS. Control of arterial branching morphogenesis in embryogenesis: go with the flow. *Cardiovasc Res* 2005;**65**:619–628.
47. Stojanović NN, Kostić A, Mitić R, Berilažić L, Radisavljević M. Association between circle of Willis configuration and rupture of cerebral aneurysms. *Medicina (Kaunas)* 2019;**55**:338.
48. Lazzaro MA, Ouyang B, Chen M. The role of circle of Willis anomalies in cerebral aneurysm rupture. *J Neurointerv Surg* 2012;**4**:22–26.
49. Liu M, Zhao J, Zhou Q, Peng Y, Zhou Y, Jiang Y. Primary cilia deficiency induces intracranial aneurysm. *Shock* 2018;**49**:604–611.
50. Rinkel GJ, Ruigrok YM. Preventive screening for intracranial aneurysms. *Int J Stroke* 2022;**17**:30–36.
51. Adil MS, Narayanan SP, Somanath PR. Cell-cell junctions: structure and regulation in physiology and pathology. *Tissue Barriers* 2021;**9**:1848212.
52. Duong CN, Vestweber D. Mechanisms ensuring endothelial junction integrity beyond VE-cadherin. *Front Physiol* 2020;**11**:519.
53. Tada Y, Yagi K, Kitazato KT, Tamura T, Kinouchi T, Shimada K, Matsushita N, Nakajima N, Satomi J, Kageji T, Nagahiro S. Reduction of endothelial tight junction proteins is related to cerebral aneurysm formation in rats. *J Hypertens* 2010;**28**:1883–1891.
54. Ponticos M, Smith BD. Extracellular matrix synthesis in vascular disease: hypertension, and atherosclerosis. *J Biomed Res* 2014;**28**:25–39.
55. Ishii T, Asuwa N. Collagen and elastin degradation by matrix metalloproteinases and tissue inhibitors of matrix metalloproteinase in aortic dissection. *Hum Pathol* 2000;**31**:640–646.
56. Aoki T, Kataoka H, Morimoto M, Nozaki K, Hashimoto N. Macrophage-derived matrix metalloproteinase-2 and -9 promote the progression of cerebral aneurysms in rats. *Stroke* 2007;**38**:162–169.
57. Kataoka K, Taneda M, Asai T, Kinoshita A, Ito M, Kuroda R. Structural fragility and inflammatory response of ruptured cerebral aneurysms. A comparative study between ruptured and unruptured cerebral aneurysms. *Stroke* 1999;**30**:1396–1401.
58. Korkmaz E, Kleinloog R, Verweij BH, Allijn IE, Hekking LHP, Regli L, Rinkel GJE, Ruigrok YM, Andries Post J. Comparative ultrastructural and stereological analyses of unruptured and ruptured saccular intracranial aneurysms. *J Neuropathol Exp Neurol* 2017;**76**:908–916.
59. Frösen J, Piippo A, Paetau A, Kangasniemi M, Niemelä M, Hernesniemi J, Jääskeläinen J. Remodeling of saccular cerebral artery aneurysm wall is associated with rupture: histological analysis of 24 unruptured and 42 ruptured cases. *Stroke* 2004;**35**:2287–2293.
60. Sieben CJ, Harris PC. Experimental models of polycystic kidney disease: applications and therapeutic testing. *Kidney360* 2023;**4**:1155–1173.
61. Tutino VM, Rajabzadeh-Oghaz H, Veeturi SS, Poppenberg KE, Waqas M, Mandelbaum M, Liaw N, Siddiqui AH, Meng H, Kolega J. Endogenous animal models of intracranial aneurysm development: a review. *Neurosurg Rev* 2021;**44**:2545–2570.
62. Makino H, Tada Y, Wada K, Liang EI, Chang M, Mobashery S, Kanematsu Y, Kurihara C, Palova E, Kanematsu M, Kitazato K, Hashimoto T. Pharmacological stabilization of intracranial aneurysms in mice: a feasibility study. *Stroke* 2012;**43**:2450–2456.
63. Hosaka K, Downes DP, Nowicki KW, Hoh BL. Modified murine intracranial aneurysm model: aneurysm formation and rupture by elastase and hypertension. *J Neurointerv Surg* 2014;**6**:474–479.
64. Barris CT, Burns-Ray E, Sullivan JC. Managing sex as a biological variable in physiological research: best practices. *Function (Oxf)* 2024;**5**:zqae034.

Downloaded from https://academic.oup.com/cardiovascres/advance-article/doi/10.1093/cvr/cvaf063/8115994 by guest on 21 May 2025